ASIAN JOURNAL OF PHARMACEUTICAL AND CLINICAL RESEARCH

INNOVARE ACADEMIC SCIENCES
Knowledge to Innovation

Vol 19, Issue 2, 2026

Online - 2455-3891
Print - 0974-2441

Research Article

GREEN SYNTHESIS OF SILVER NANOPARTICLES FROM NEEM BARK FOR THE REMEDIATION OF WATERBORNE PATHOGENS

JANHAVI HARISH INDURKAR[1]*, ARCHANA NISCHAL MUNGLE[1], GULSHAN GURUNANI[1], SHUBHAM KAMBLE[2], SHUBHAM S GUPTA[3], AKSHAY VIJAY RAMTEKE[4], NISCHAL P MUNGLE[5]

[1]Department of Pharmaceutical Chemistry, Gurunanak College of Pharmacy, Nagpur, Maharashtra, India. [2]Department of Pharmaceutics, Kamla Nehru College of Pharmacy, Butibori, Maharashtra, India. [3]Department of Pharmaceutical Sciences, Gurunanak College of Pharmacy, Nagpur, Maharashtra, India. [4]Department of Pharmaceutics, Central India College of Pharmacy, Nagpur, Maharashtra, India. [5]Department of Mechanical Engineering, Yeshawantrao Chavan College of Engineering, Nagpur, Maharashtra, India.
***Corresponding author: Janhavi Harish Indurkar; Email: janhaviindurkar478@gmail.com**

Received: 02 June 2025, Revised and Accepted: 24 December 2025

ABSTRACT

Objective: The objective of the study was to develop an eco-friendly method for synthesizing silver nanoparticles (AgNPs) using neem (*Azadirachta indica*) bark extract as a reducing and stabilizing agent, and to evaluate their antibacterial, antipathogenic, and larvicidal activities for water purification and vector control.

Methods: AgNPs were synthesized by green chemistry using neem bark (NB) extract, avoiding hazardous chemicals. Synthesis parameters – pH, temperature, and reaction time – were optimized. Characterization included ultraviolet (UV)-Visible spectroscopy (Shimadzu UV-1800), Fourier transform infrared (Perkin Elmer Spectrum-One, USA), X-ray diffraction (Cu Kα radiation, λ = 1.5406 Å), SEM (Hitachi S-3400N), TEM (JEOL-JEM-2100F, 200 kV), particle size analysis, and zeta potential measurement. Antibacterial activity against *Staphylococcus aureus* and *Escherichia coli* was tested by the well diffusion method. Antipathogenic activity was assessed using pathogenic sewer water, and larvicidal activity was evaluated against mosquito larvae (n=10/concentration).

Results: Spherical NB AgNPs (40–150 nm) with a characteristic SPR peak at 425 nm were obtained. X-ray diffraction confirmed a face-centered cubic crystalline structure with an average crystallite size of 7.66 nm. Zeta potential values (–26.7 to –33.2 mV) indicated good colloidal stability. Antibacterial testing showed maximum inhibition zones of 47 mm for *S. aureus* and 37 mm for *E. coli* at 25 µg/mL. In pathogenic water, smaller particles exhibited higher inhibition efficiency. Larvicidal assays achieved 100% mortality at 2.5 µg/mL within 3 h ($p<0.05$), with no mortality in controls.

Conclusion: NB -mediated AgNPs demonstrate strong antibacterial, antipathogenic, and larvicidal properties, making them a low-cost, sustainable option for water purification and mosquito control. Further studies should focus on *in vivo* performance, environmental safety, and large-scale application.

Keywords: Silver, Nanoparticles, Neem, Azadirachta, Biosynthesis, Green, Antibacterial, Antipathogenic, Larvicidal, Water Purification, Vector, Control, Ecofriendly, Stability, Crystalline, Characterization, Pathogens, Mosquito, Sustainability.

 DOI: http://dx.doi.org/10.22159/ajpcr.2026v19i2.55385. Journal homepage: https://innovareacademics.in/journals/index.php/ajpcr

INTRODUCTION

As of 2022, around 1.7 billion people globally rely on drinking water contaminated with feces, posing major health risks. Waterborne pathogens can cause diseases like cholera, typhoid, and diarrhea, leading to approximately 505,000 diarrheal deaths annually. In 2021, over 2 billion people lived in water-stressed regions, a figure expected to rise due to climate change and population growth. While 73% of the global population had access to safely managed drinking water in 2022, significant gaps remain in water quality and availability. In the developing world, particularly in rural and poor communities, some 35% of the people suffer from water-related diseases because of the absence of water treatment facilities [1]. To combat this critical issue, there is an increasing demand for low-cost and low-energy-consuming water purification processes. Nanotechnology provides an ideal approach, if not a solution, and nanoparticles (NPs), with their special properties as a result of nanoscale dimensions (1–100 nm), huge surface area and high chemical reactivity, are promising tools as sensors which can play very crucial roles [2] of these, silver nanoparticles (AgNPs) are particularly attractive due to their strong antimicrobial and catalytic properties, and the relatively low toxicity toward human beings [3]. The green method for the synthesis of AgNPs is the eco-friendly approach in which green reducing agents (plant extracts) are used to convert the metal salt into stable NPs [4]. This process employs neem (*Azadirachta indica*) bark extract, which is a source of bioactive compounds, acting both as a reducing and stabilizing agent. Flavonoids, terpenoids, alkaloids, enzymes, and other compounds are mainly responsible for the nucleation of the NPs as well as functionalization. The two-step mechanism of NB-AgNPs biosynthesis by neem bark (NB) extract: In nucleation phase, silver ions reduce and an atomic clusters are formed, and then after some time they proceed and in growth phase, these clusters aggregate to produce different shape and size of NPs. The high reduction potential of silver makes it possible to produce stable NPs even in aqueous solution without adding external stabilizing agents [6]. Key synthesis parameters, including temperature, pH, reaction time, and extract concentration, exert a great influence on the particle size, morphology, and antimicrobial activity of the resulting NB-AgNPs. Hence, the present work aimed at optimizing the experimental conditions for a greener synthesis of NB-mediated AgNPs s and assessing their potential antimicrobial activity toward waterborne pathogens. The findings underscore the suitability of neem-based NB-AgNPs as an eco-friendly and cost-effective alternative to restore water quality and minimize the health crisis caused by unsafe water.

METHODS

Collection and authentication of plant material

The bark of *A. indica* (commonly known as Neem) was collected from the premises of Gurunanak College of Pharmacy, located in Nagpur, Maharashtra, India, at the geographical coordinates of 21.146633° N latitude and 79.0882° E longitude. The selection of this location ensured that the plant material was sourced from a clean, monitored environment, minimizing potential contamination. Immediately after collection, the bark samples were subjected to a thorough cleaning process. This involved initially washing the bark with tap water to eliminate visible dirt, debris, and other surface contaminants. Subsequently, the samples were rinsed with distilled water to ensure the removal of any residual impurities and to maintain the purity required for downstream applications, particularly in NP synthesis. Following the cleaning process, the bark was air-dried under shade at ambient room temperature (approximately 25–30°C) for a duration of 6–7 days. Shade drying was preferred over sun drying to preserve the integrity of the bioactive compounds present in the bark, which might otherwise degrade upon exposure to direct sunlight or elevated temperatures. For scientific validation, the botanical identity of the *A. indica* bark was authenticated by the Department of Botany, Rashtrasant Tukadoji Maharaj Nagpur University, Nagpur. The plant specimen was officially verified and assigned the reference specimen number 462, ensuring accurate taxonomic classification for future reference.

Procurement of Materials and Instrument used

Silver nitrate ($AgNO_3$), Mueller-Hinton agar medium, and nutrient agar were obtained from HiMedia Laboratories Pvt. Ltd., Mumbai, India. Ethanol was sourced from Chungshu Hongsheng Fine Chemical Co., Ltd., and deionized (DI) water from Merck Life Sciences Pvt. Ltd., Mumbai. NB was collected from the premises of Gurunanak College of Pharmacy, Nagpur. All reagents were of analytical grade. *Escherichia coli* and *Staphylococcus aureus* strains were used for antimicrobial studies, while mosquito larvae and pathogenic water samples were collected from household coolers and local sewage, respectively. Experimental analyses employed a ultraviolet–visible (UV-Vis) spectrophotometer (UV-1800, Shimadzu Corporation, Kyoto, Japan) for absorbance measurements and an analytical balance (AUY-220, Shimadzu Corporation, Kyoto, Japan) for weighing samples. A magnetic stirrer (Model 1MLH, REMI, India) was used for solution mixing, and Fourier transform infrared (FTIR) spectra were recorded using an IR Affinity spectrophotometer (Shimadzu Corporation, Kyoto, Japan). Centrifugation was carried out with a cooling centrifuge (REMI, India). Particle size distribution and zeta potential were determined using a Zeta Sizer (Malvern Panalytical, Malvern, United Kingdom) and a particle size analyzer (Shimadzu Corporation, Kyoto, Japan). Surface morphology was examined using a scanning electron microscope (SEM; model as available), and crystalline structure was analyzed with a powder X-ray diffractometer (Bruker Corporation, Germany).

Preparation of alcoholic bark extract

The NB was thoroughly washed with tap water and then rinsed with distilled water to remove any dust and impurities [5]. Afterward, the bark was shade-dried at room temperature for 6–7 days. Once dried, the bark was ground into a coarse powder. A total of 266.53 g of the powdered bark was transferred to an airtight container for cold maceration, followed by the addition of 1 L of ethanol. The mixture was left to macerate for 15 days, with frequent stirring every 2 days. After 15 days, the extract was filtered through muslin/cotton cloth, collected in Petri dishes, and allowed to dry for 24 h [6]. This method was adapted from the procedure reported by Kitimu *et al*. (2022).

Green Synthesis of NB-AgNPs Using NB Extract

A 1 mM aqueous solution of $AgNO_3$ was prepared in an Erlenmeyer flask, and the pH was adjusted to 8. A stock solution of NB extract was prepared by dissolving 100 mg of the powdered extract in 100 ml of ethanol. To prepare the working solution, 10 ml of the stock solution was diluted with ethanol to a final volume of 100 ml. The extract solution was then added to the $AgNO_3$ solution in a 1:9 (v/v) ratio at room temperature. The mixture was heated on a magnetic stirrer with a thermostat, maintaining the temperature between 60 and 80°C. The color change of the solution was observed at 10-min intervals over a period of up to 1 h. To confirm the synthesis of AgNPs, UV-Vis spectrophotometry analysis was performed starting 3 h after the reaction began, and continued at intervals up to 24 h.

Optimization of green synthesis of AgNPs

To optimize the synthesis conditions of NB-AgNPs, the effects of both reaction time and temperature were investigated. The alcoholic NB extract was mixed with a 1 mM $AgNO_3$ solution in a 1:9 (v/v) ratio. For time optimization, the reaction was monitored over a 24-h period to assess NP formation. To evaluate the impact of temperature, the reaction mixture was subjected to different thermal conditions, including room temperature and elevated temperatures ranging from 60°C to 80°C, to determine the most favorable temperature range for efficient NB-AgNP synthesis.

CHARACTERIZATION OF GREEN SYNTHESIZED AGNPS

UV-Vis spectroscopy

The synthesized AgNPs appeared as solid particles exhibiting a characteristic dark brown color (Fig. 1), indicating successful formation. Preliminary confirmation of the NP was carried out using UV-Vis spectroscopy with a Shimadzu UV-1800 spectrophotometer. Optical density (OD) measurements of the colloidal solution (1 mL) were taken at regular intervals, starting at 3 h and continuing up to 24 h. Ethanol was used as the blank for calibration. The absorbance spectra were recorded within the wavelength range of 300–700 nm to identify the characteristic surface plasmon resonance peak associated with AgNPs [7].

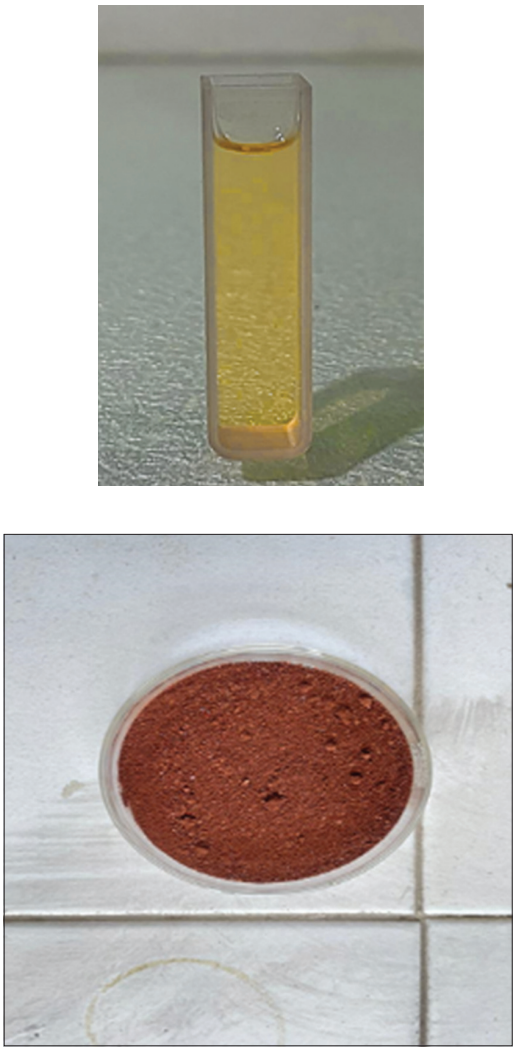

Fig. 1: Illustrating synthesized silver nanoparticles appeared as solid particles exhibiting a characteristic dark brown color

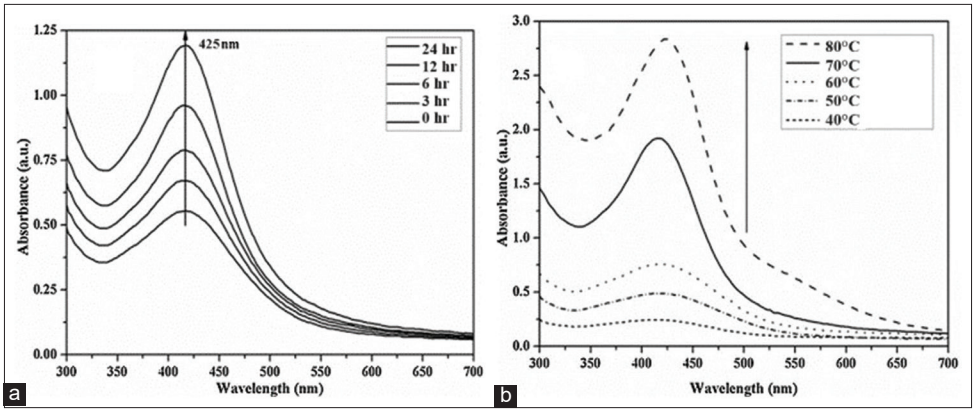

Fig. 2: (a) Ultraviolet visible (UV-Vis) absorbance of neem bark-mediated silver nanoparticles at various time intervals. (b) UV-Vis spectra of neem bark mediated Silver nanoparticles at various temperatures

Particle size analysis and zeta potential measurement

The mean particle size and polydispersity index of both solid and liquid batches of synthesized AgNPs were measured using photon correlation spectroscopy (PCS), with 2 mL of sample placed in a quartz cell and readings taken at a 90° angle in triplicate. Surface zeta potential was determined using a laser zeta meter. For this, 5 mL of NP suspension was diluted with 50 mL of double-distilled water containing 2×10^{-2} M NaCl as the electrolyte. The pH was adjusted, and samples were shaken for 30 min before recording the equilibrium pH and measuring the zeta potential. Each result represents the average of three measurements [8].

FTIR spectroscopy of green-synthesized AgNPs

FTIR spectroscopy was performed to identify functional groups capping the AgNPs. The synthesized solution was centrifuged at 10,000 rpm for 30 min, and the resulting pellet was redispersed, dried, and analyzed using a Perkin Elmer Spectrum-One FTIR instrument (USA). Spectra were recorded in the range of 4000–400 cm^{-1} [9].

X-ray diffraction (XRD) analysis

XRD was used to assess the crystalline nature of the green-synthesized NB-AgNPs. Dried NP powder was deposited on glass slides and analyzed using Cu Kα radiation (λ = 1.5406 Å) at 30 kV and 40 mA, with a nickel monochromator. Scanning was performed in the 2θ range of 10°–90° [10]. The average crystallite size was calculated using Scherrer's equation:

$$D = \frac{0.94\lambda}{(\beta \cos\theta)}$$

where D is the crystallite size, λ is the X-ray wavelength, θ is Bragg's angle, and β is the FWHM in radians.

Scanning electron microscopy of green synthesized AgNPs

The surface morphology of the NP was examined using scanning electron microscopy (SEM). Dry NP samples were prepared by applying a drop onto a carbon-coated grid, which was allowed to dry before measurement on a Hitachi S-3400 N SEM instrument. The SEM instrument operated at an accelerated voltage of 20 kV [11].

SEM-energy-dispersive X-ray (EDX)

The presence of elemental silver was confirmed through energy dispersive spectroscopy [12]. EDX analysis was carried out for dried NPs exposed and coated onto carbon film, performed on a Scanning Electron Microscopy instrument equipped with Thermo EDX attachments. Thin films of the sample were prepared on a carbon-coated copper grid by dropping a small amount of the sample on the grid, and then the film on the SEM grid was allowed to dry by exposure under a mercury lamp for 5 min [13].

Fig. 3: The physical appearance of silver nitrate, alcoholic neem bark solution, and silver nanoparticles from neem bark extract

TEM analysis

The size, shape, and morphology of the biosynthesized AgNPs were determined using a transmission electron microscopy (TEM). The samples for the TEM were prepared by sonicating the pellet of centrifuged Ag-NPs in DI water. A drip ofthehomogeneoussuspensio nwasplacedonacarbon-coatedcoppergridwithalacey carbon film and allowed to dry at room temperature [14]. The images (Fig. 2) were collected using a field emission JEOL-JEM-2100F TEM operating at 200 KV (JEOL, Tokyo, Japan).

Anti-microbial activity of green-synthesized AgNPs

To assess the antimicrobial activity of the green-synthesized AgNPs, bacterial strains were grown overnight in nutrient broth at 37°C. Nutrient agar plates were prepared, and 100 µL of bacterial inoculum (*E. coli* and *S. aureus*) was spread evenly across the surface using sterile cotton swabs. Wells of 7 mm diameter were then created in the agar using a sterile gel borer. Different concentrations of NB-AgNPs (20, 40, 60, 80, and 100 µg/mL) were added to the wells (100 µL/well) showed in Graph 1. The plates were incubated at 37°C for 24 h, and the zones of inhibition surrounding each well were measured and recorded (Fig. 10) [15].

Pathogenic water activity of green-synthesized AgNPs

To evaluate the anti-pathogenic activity of green-synthesized AgNPs, Mueller-Hinton Agar plates were prepared, and 100 µL of pathogenic water samples were uniformly spread using sterile cotton swabs. Wells with a diameter of 7 mm were created using a sterile gel borer. Into each well, 100 µL of NB-AgNPs at varying concentrations (20, 40, 60, 80, and 100 µg/mL) were introduced. The plates were then incubated at 37°C for 24 h. After incubation, the zones of inhibition around each well were measured to assess the NPs' effectiveness against waterborne pathogens [16].

Table 1: Interpretation of FTIR spectra of NB extract and NB-NB-AgNPs

Peak (cm^{-1}) – NB extract	Peak (cm^{-1}) – NB-NB-AgNPs	Bond type	Inference/Remarks
3244.54	3301.19/3747.69	O–H Stretching (Alcohols, Phenols)	Presence of alcohols/phenols; broad peaks indicate strong hydrogen bonding
2922.16/2852.72	2922.16/2852.72	C–H Stretching (Alkanes)	Presence of methylene (–CH_2–) groups; common in organic compounds
–	2135.2	C≡C Stretching (Alkynes)	Triple-bonded carbon structures (alkynes)
1743.01	1734.01	C=O Stretching (Carbonyl Compounds)	Presence of esters, aldehydes, or ketones; sharp peak shows strong carbonyl presence
–	1888.31	C=O Stretching (Conjugated Systems)	Indicates carbonyl in conjugated systems
1649.14	1649.14	C=C Stretching (Alkenes)	Presence of alkenes; double-bonded carbon
1450.26/1374.01	1456.26/1363.67	C–H Bending (Alkanes)	Typical bending vibrations of alkanes
1246.52	1101.35	C–O Stretching (Alcohols, Ethers)	Strong peaks indicating presence of alcohols, ethers, or esters
831.32/720.46	831.32/723.31	C–H Bending (Aromatic Compounds)	Presence of aromatic ring structures
–	569.00/476.42	Metal–Oxygen Bonds	Indicates Ag–O interactions; confirms nanoparticle formation and capping by biomolecules

FTIR: Fourier transform infrared, NB: Neem bark, AgNPs: Silver nanoparticles

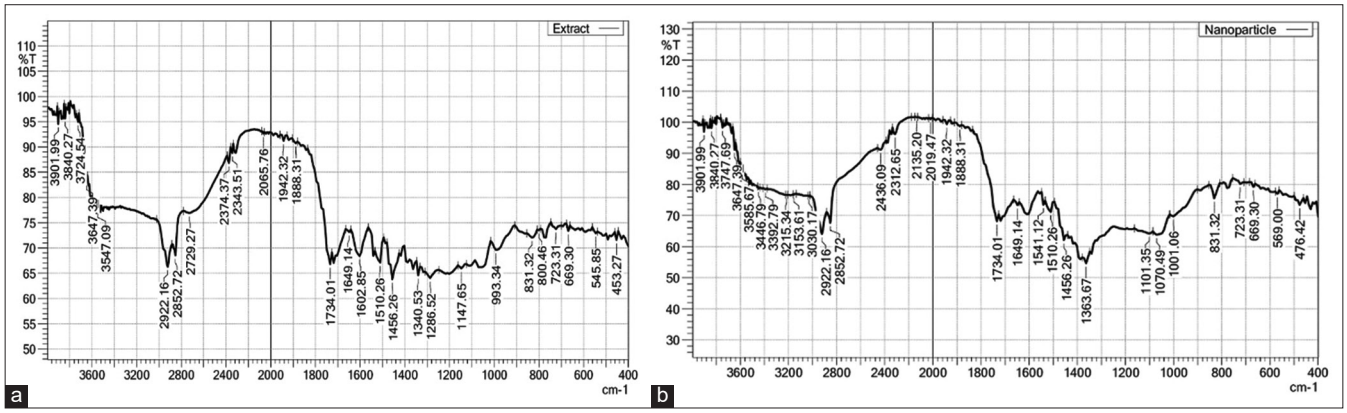

Fig. 4: (a) Fourier transform infrared (FTIR) graph of neem bark (NB) extract (b) FTIR graph of NB-NB-silver nano particles

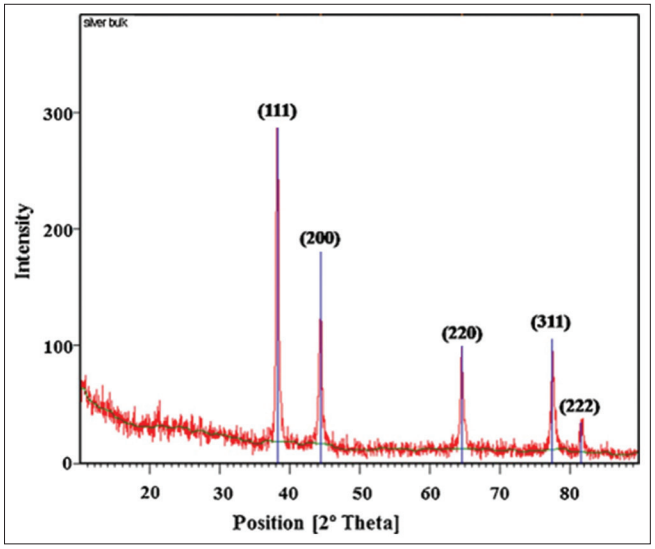

Fig. 5: X-ray diffraction pattern of synthesized nanoparticles

Larvicidal activity of green-synthesized AgNPs

To assess the larvicidal activity of the green-synthesized AgNPs, mosquito eggs collected from household coolers were cultured under standard laboratory conditions. Bioassays were conducted using NB-AgNP test solutions prepared at concentrations of 10, 20, 30, 40, and 50 µg/mL. For each concentration, corresponding controls containing only distilled water and NB extract (without NB-AgNPs) were included. Ten mosquito larvae were placed into China dishes containing 10 mL of each test solution and maintained at room temperature. Larval mortality was observed over time, with death confirmed when no movement occurred upon gentle probing with a needle. The percentage mortality at each concentration was calculated and compared to control groups to determine the efficacy of the NB-AgNPs [17].

RESULTS

Characterization of biosynthesized NB-AgNPs

The green synthesis of NB-AgNPs using *A. indica* (neem) bark extract was confirmed through a series of advanced characterization techniques, validating the successful formation of bio-functionalized NPs with varied sizes, shapes, and morphologies. The initial indication of NB-AgNP formation was observed as a visible color change in the reaction mixture from colorless to dark brown Illustrated in Fig. 3 which signifying the reduction of Ag^+ ions, which corresponded to a surface plasmon resonance (SPR) peak at 425 nm, as detected by UV-Vis spectrophotometry, as illustrated in Fig. 2. FTIR analysis as illustrated in Fig. 4 of the NB extract and the synthesized NB-AgNPs revealed key functional groups, including O–H, C–H, C=O, C=C, and aromatic rings. Additional peaks attributed to C≡C stretching and metal-oxygen interactions indicated the involvement of these biomolecules in the reduction and stabilization processes mention in Table 1. XRD analysis confirmed the crystalline nature of the NPs, with sharp peaks at 2θ values of 38.2°, 44.4°, 64.5°, and 77.6°, characteristic of a face-centered cubic silver structure. The average crystallite size, calculated using the Scherrer equations illustrated in Fig. 5, was approximately 7.66 nm. Particle size distribution, measured by PCS, revealed average sizes of 122.71 nm in the liquid batch and 152 nm in the solid batch, illustrated

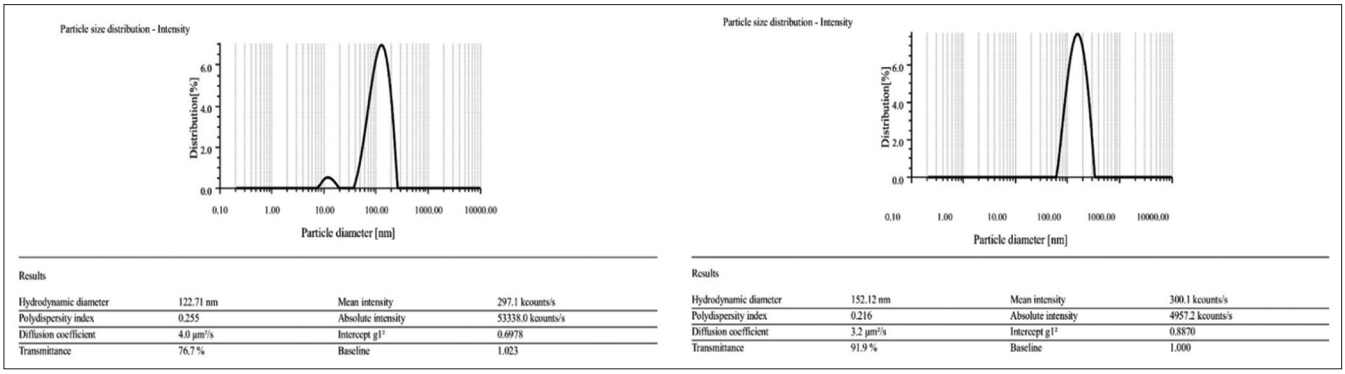

Fig. 6: (Batch A-liquid): Particle size of the synthesized neem bark (NB)-NB-silver nanoparticles (AgNPs), (Batch B-solid): Particle size of the synthesized NB-NB-AgNPs

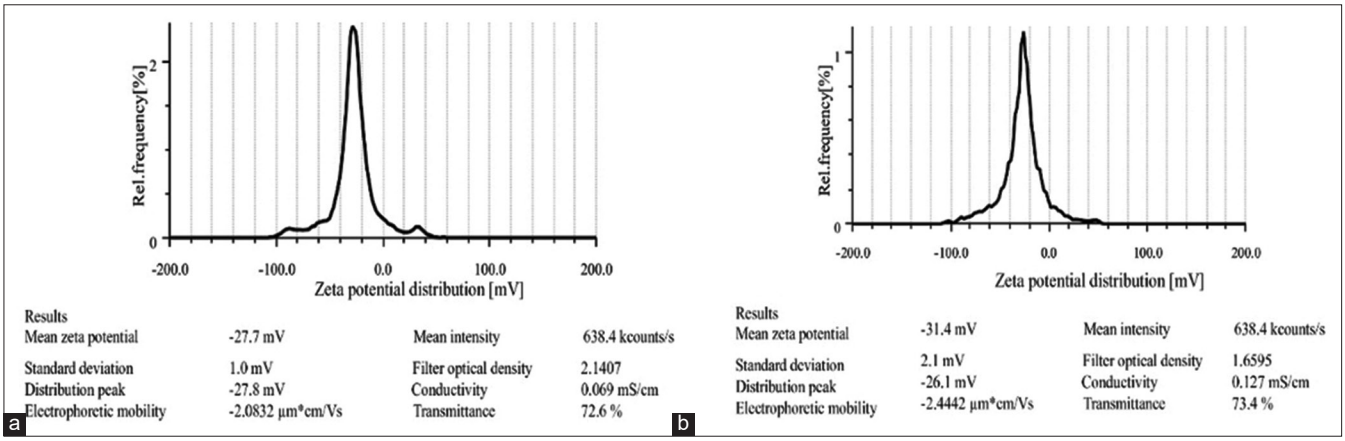

Fig. 7: (a) Zeta potential of Sample A- Liquid, (b): Zeta potential of Sample B- Solid

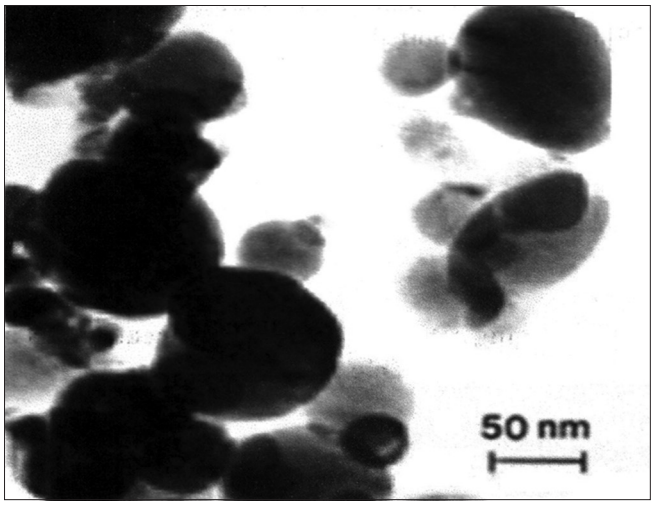

Fig. 8: TEM images of biosynthesized silver nanoparticles

in Fig. 6. Zeta potential values ranging from –26.7 mV to –31.4 mV indicated good colloidal stability as illustrated in Fig. 7, attributed to effective capping by phytochemicals from the neem extract. Scanning electron microscopy (SEM) analysis demonstrated uniformly spherical NB-AgNPs with average sizes of 58.11 nm and 43.95 nm across two batches as illustrated in Fig. 8. Complementarily, transmission electron microscopy (TEM) revealed well-dispersed, predominantly spherical NPs with high morphological uniformity and sizes ranging from 40 to 150 nm, as illustrated in Fig 9, consistent with the SPR band observed in UV-Vis analysis. Dynamic Light Scattering (DLS) further supported this by showing size distribution peaks with a dominant average diameter

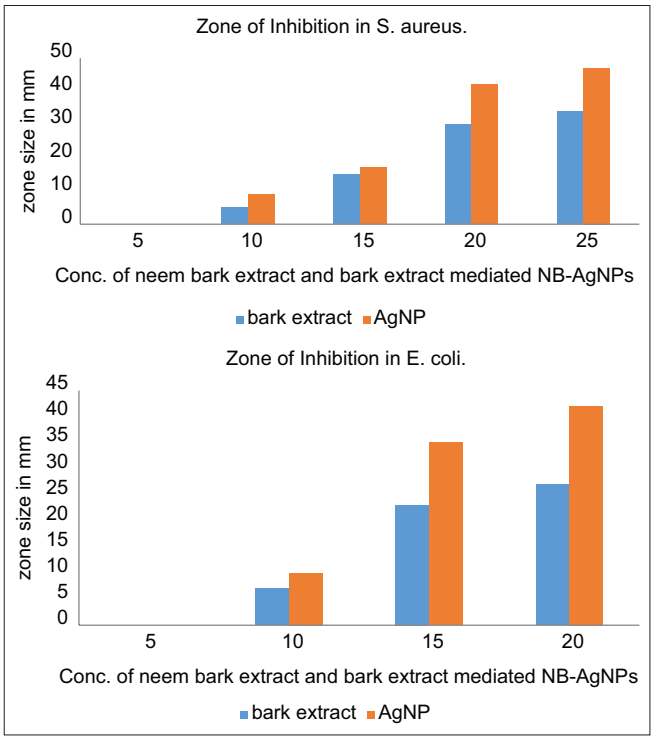

Graph 1: Different zone sizes exhibited by *Escherichia coli*, Different zone sizes exhibited by *Staphylococcus aureus*

of 38.5 nm (86.4%) and a smaller fraction at 6.5 nm (13.6%), along with a zeta potential of –33.2 mV, reinforcing the high stability of the colloidal

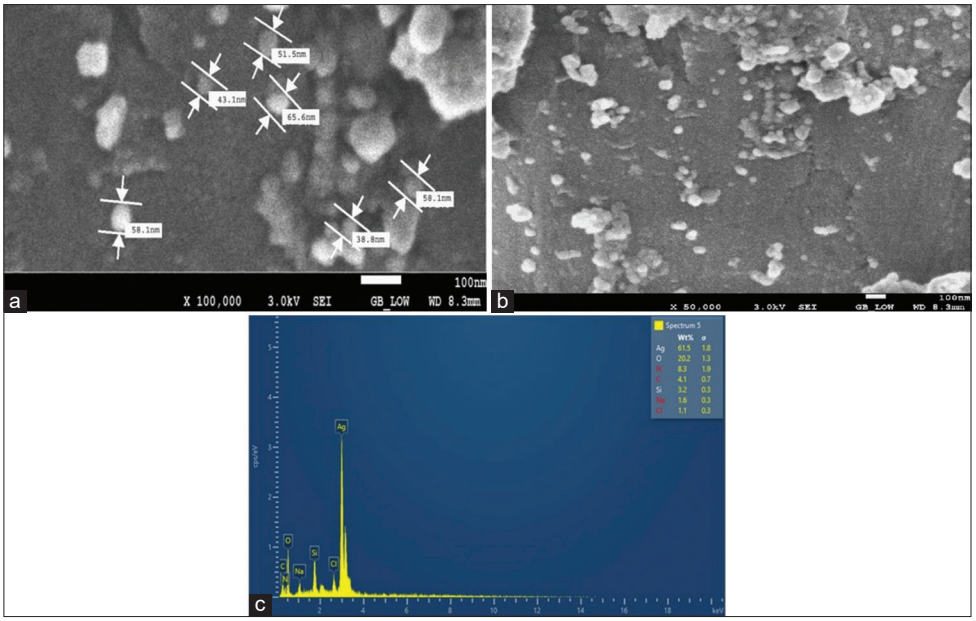

Fig. 9: (a) SEM graph of the neem bark (NB)-NB-silver nanoparticles (AgNPs) and (b) Energy-dispersive X-ray graph of the synthesized NB-AgNPs

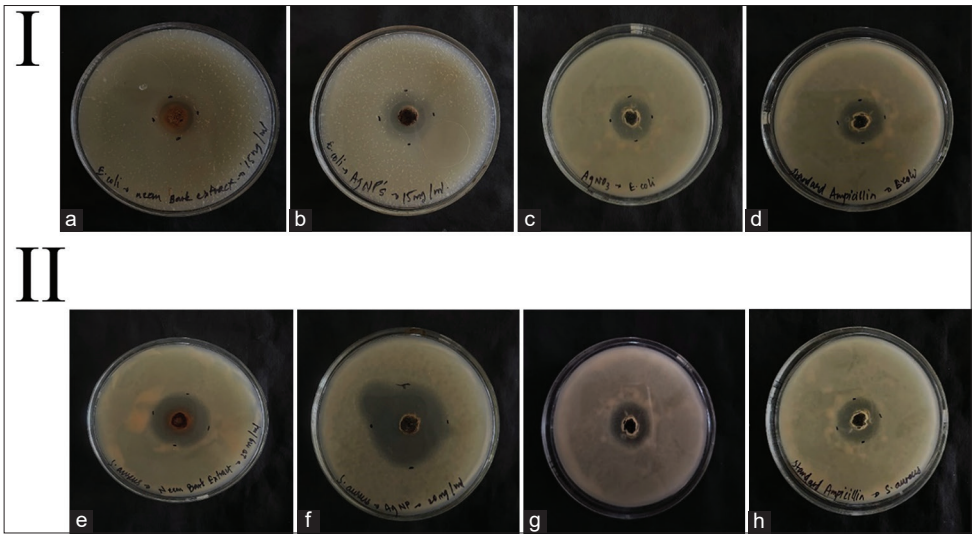

Fig. 10: I-Zones of inhibition in *Escherichia coli*: (a) (Neem bark [NB] extract) (b) (NB-silver nanoparticles [AgNPs]) (c) (silver nitrate [$AgNO_3$]), and (d) (standard Ampicillin), II-Zones of inhibition in *E. coli*: (e) (neem bark extract), (f) (NB-AgNPs), (g) ($AgNO_3$), and (h) (standard ampicillin)

Fig. 11: Illutration of bioassay of larvicidal activity (water and neem bark [NB] extract)

system. EDX spectroscopy confirmed the elemental composition, with a strong silver signal at 3 keV and additional peaks for oxygen, nitrogen, carbon, chlorine, sodium, and silicon. The presence of Cl and Si was likely due to residual moisture from the plant extract and minor contamination from borosilicate glassware. Collectively, these results confirm the successful green synthesis of stable, well-characterized, biofunctionalized AgNPs using NB extract, with promising properties for further biological and environmental applications.

BIOFUNCTIONAL PROPERTIES OF AgNPs SYNTHESIZED USING NB EXTRACT

Antibacterial activity

Green-synthesized NB-AgNPs were tested against *S. aureus* and *E. coli* using the disk diffusion method at concentrations of 5–25 µg/mL mentioned in Table 2.*E. coli* showed inhibition at 15 µg/mL, while *S. aureus* responded at 20 µg/mL, with the latter

Table 2: Comparative antibacterial activity of green-synthesized NB-AgNPs, neem extract, and silver nitrate against *S. aureus* and *E. coli*

Bacteria	Type	Concentration	Zone of Inhibition (NB-AgNPs) (mm) Mean±SD	Zone of Inhibition (Neem extract) (mm) Mean±SD	Zone of Inhibition (silver nitrate) (mm) Mean±SD
S. aureus	Gram-positive	5 µg/mL	0±0 (n=3)	0±0 (n=3)	—
S. aureus	Gram-positive	10 µg/mL	9±0.5 (n=3)	7±0.3 (n=3)	—
S. aureus	Gram-positive	15 µg/mL	17±0.6 (n=3)	15±0.5 (n=3)	—
S. aureus	Gram-positive	20 µg/mL	42±1.0 (n=3)	30±0.7 (n=3)	—
S. aureus	Gram-positive	25 µg/mL	47±1.2 (n=3)	34±0.8 (n=3)	—
S. aureus	Gram-positive	1 mM	—	—	23±0.6 (n=3)
E. coli	Gram-negative	5 µg/mL	0±0 (n=3)	0±0 (n=3)	—
E. coli	Gram-negative	10 µg/mL	10±0.4 (n=3)	7±0.2 (n=3)	—
E. coli	Gram-negative	15 µg/mL	35±0.9 (n=3)	23±0.6 (n=3)	—
E. coli	Gram-negative	20 µg/mL	37±1.0 (n=3)	27±0.7 (n=3)	—
E. coli	Gram-negative	25 µg/mL	—	—	—
E. coli	Gram-negative	1 mM	—	—	20±0.5 (n=3)

Data presented as Mean±SD. n: Number of experiments, *E. coli: Escherichia coli, S. aureus: Staphylococcus aureus*, NB: Neem bark, AgNPs: Silver nanoparticles, SD: Standard deviation

Table 3: Larvicidal activity of deionized water (control), aqueous extract of *Azadirachta indica* leaves, and extract-mediated NB-AgNPs at different concentrations against mosquito larvae

Time	Control (Water) Mean±SD	NB extract Mean±SD	NB-AgNPs 0.5 µg/mL Mean±SD	NB-AgNPs 1.0 µg/mL Mean±SD	NB-AgNPs 1.5 µg/mL Mean±SD	NB-AgNPs 2.0 µg/mL Mean±SD	NB-AgNPs 2.5 µg/mL Mean±SD
15 min	0±0 (n=3)	0±0 (n=3)	0±0 (n=3)	0±0 (n=3)	0±0 (n=3)	0±0 (n=3)	0±0 (n=3)
30 min	0±0 (n=3)	0±0 (n=3)	0±0 (n=3)	0±0 (n=3)	0±0 (n=3)	0±0 (n=3)	0±0 (n=3)
45 min	0±0 (n=3)	0±0 (n=3)	20±0.4 (n=3)	20±0.4 (n=3)	25±0.5 (n=3)	30±0.6 (n=3)	30±0.6 (n=3)
60 min	0±0 (n=3)	0±0 (n=3)	20±0.4 (n=3)	25±0.5 (n=3)	25±0.5 (n=3)	30±0.6 (n=3)	35±0.6 (n=3)
1 h 30 min	0±0 (n=3)	0±0 (n=3)	25±0.5 (n=3)	35±0.6 (n=3)	40±0.7 (n=3)	40±0.7 (n=3)	60±0.8 (n=3)
2 h	0±0 (n=3)	0±0 (n=3)	30±0.6 (n=3)	40±0.7 (n=3)	50±0.8 (n=3)	65±0.9 (n=3)	85±1.0 (n=3)
3 h	0±0 (n=3)	0±0 (n=3)	40±0.7 (n=3)	60±0.8 (n=3)	80±0.9 (n=3)	85±1.0 (n=3)	100±0.0 (n=3)

Data presented as Mean±SD. n: Number of experiments, NB: Neem bark, AgNPs: Silver nanoparticles, SD: Standard deviation

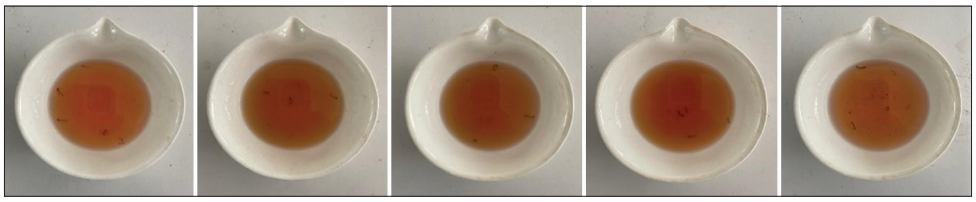

Fig. 12: A representative display of larvicidal bioassay, using Water (control), *Azadirachta indica* extract, and neem bark-silver nanoparticles in various concentrations

showing the largest inhibition zone. NB-AgNPs were more effective against Gram-positive bacteria, likely due to differences in cell wall structure. Their nanoscale size allows them to attach to and penetrate bacterial membranes, disrupting respiration and leading to cell death.

Antipathogenic activity (pathogenic water)

The anti-pathogen activity of green-synthesized NB-AgNPs was tested on sewer-sourced pathogenic water using the well diffusion method. NB-AgNPs showed strong antibacterial effects, with inhibition zones varying based on the concentration of NB extract used in synthesis. Higher extract concentrations produced smaller NPs, which exhibited greater antibacterial activity due to their larger surface area. These NPs adhered to and penetrated bacterial membranes, disrupting respiration and causing cell death. The results highlight the potential of eco-friendly NB-AgNPs for treating contaminated water and addressing waterborne health risks.

Larvicidal activity

The larvicidal activity of *A. indica* (neem) alcoholic extracts and their NB-AgNPs was tested against mosquito larvae. At 0 h, larvae in all samples were actively moving. After 3 h, no mortality was observed in the control or neem extract samples. However, NB-AgNP-treated groups showed concentration-dependent mortality: 0.5, 1.0, 1.5, 2.0, and 2.5 µg/mL resulted in 40%, 60%, 80%, 85%, and 100% mortality, respectively. Dead larvae appeared curled or clustered, indicating the strong larvicidal potential of NB-AgNPs compared to the crude extract.

Table 3 presents the larvicidal activity of green-synthesized AgNPs at different concentrations (0.5 to 2.5 µg/mL) over time, compared to control groups (water and NB extract). Larval mortality was assessed at intervals up to 3 h. At the beginning (15 and 30 min), no mortality was observed in any sample (Figs. 11 and 12). From 45 min onward, AgNPs began to show a concentration-dependent increase in larval mortality. By the 3-h mark, the highest concentration (2.5 µg/mL) achieved 100% mortality, while lower concentrations showed progressively less effect. Neither the water control nor the NB extract alone caused any larval death throughout the experiment. This data demonstrates the significant and dose-dependent larvicidal effect of AgNPs, with increasing mortality over time, highlighting their potential as an effective bio-control agent.

CONCLUSION

The present study successfully established a green and eco-friendly method for the synthesis of AgNPs using *A. indica* (neem) bark extract, which served the dual purpose of reducing and stabilizing the NPs. This approach not only aligns with the principles of green chemistry by eliminating the need for hazardous chemicals and energy-intensive processes but also utilizes a widely available and sustainable plant

resource. Comprehensive characterization through UV-Vis spectroscopy, FTIR, XRD, SEM, TEM, particle size analysis, and zeta potential confirmed the successful formation of stable, biofunctionalized AgNPs with predominantly spherical morphology and sizes ranging from 40 to 150 nm. These NPs exhibited good dispersion and long-term stability due to surface capping by phytochemicals such as flavonoids, terpenoids, and alkaloids inherently present in the NB. Functionally, the NB-AgNPs demonstrated significant bioactivity across multiple domains. They showed strong antibacterial properties against both Gram-positive (*S. aureus*) and Gram-negative (*E. coli*) bacteria, with enhanced activity against *S. aureus*, likely due to structural differences in bacterial cell walls. The NB-AgNPs also exhibited potent antimicrobial action against pathogens in contaminated sewer water, indicating their potential in low-cost and sustainable water purification systems. Moreover, the synthesized NPs displayed excellent larvicidal efficacy against mosquito larvae, achieving complete mortality within 3 h at a low concentration, highlighting their promise for use in vector control strategies aimed at combating mosquito-borne diseases such as malaria and dengue. Overall, the study underscores the multifunctionality of NB -mediated AgNPs as an effective and environmentally benign nanomaterial with broad-spectrum applications in public health and environmental safety. Future directions should include *in vivo* studies, environmental toxicity assessments, and the development of user-friendly formulations to facilitate their integration into practical applications such as antibacterial coatings, water filtration units, and larvicidal agents.

AUTHOR CONTRIBUTATIONS

J.H.I. contributed to conceptualization, investigation, project administration, supervision, validation, writing–original draft, and writing–review & editing; A.N.M. contributed to investigation, methodology, data curation, and writing–review and editing; G.G. contributed to investigation, data curation, and formal analysis; S.K. contributed to methodology, validation, and writing–review & editing; S.S.G. contributed to data curation, formal analysis, and visualization; A.V.R. contributed to investigation, resources, and data curation; N.P.M. contributed to supervision, project administration, and critical review of the manuscript.

CONFLICTS OF INTEREST

The authors declare no conflicts of interest

REFERENCES

1. World Health Organization. Drinking-water [Internet]. Geneva: WHO; 2023 Sep 13. [cited May 26 2025] Available from: https://www.who.int/news-room/fact-sheets/detail/drinking-water.
2. Melkani I, Kumar B, Pandey NK, Singh S, Baghel DS, Sudhakar K. Therapeutic impact of nanomedicine for the treatment of neuropathic pain: principle, prospective and future. Int J Appl Pharm. 2024;16(5):46-58. doi: 10.22159/ijap.2024v16i5.50457.
3. Nie P, Zhao Y, Xu H. Synthesis, applications, toxicity and toxicity mechanisms of silver nanoparticles: a review. Ecotoxicol Environ Saf. 2023;253:114636. doi: 10.1016/j.ecoenv.2023.114636, PMID 36806822.
4. Shahzadi S, Fatima S, Ul Ain Q, Shafiq Z, Janjua MR. A review on green synthesis of silver nanoparticles (SNPs) using plant extracts: a multifaceted approach in photocatalysis, environmental remediation, and biomedicine. RSC Adv. 2025;15(5):3858-903. doi: 10.1039/d4ra07519f, PMID 39917042.
5. Asimuddin M, Shaik MR, Adil SF, Siddiqui MR, Alwarthan A, Jamil K *et al*. Azadirachta indica based biosynthesis of silver nanoparticles and evaluation of their antibacterial and cytotoxic effects. J King Saud Univ Sci. 2020;32(1):648-56. doi: 10.1016/j.jksus.2018.09.014.
6. Kitimu SR, Kirira P, Abdille AA, Sokei J, Ochwang'i D, Mwitari P *et al*. Anti-angiogenic and anti-metastatic effects of biogenic silver nanoparticles synthesized using Azadirachta indica. Adv Biosci Biotechnol. 2022;13(4):188-206. doi: 10.4236/abb.2022.134010.
7. Ansari M, Ahmed S, Abbasi A, Khan MT, Subhan M, Bukhari NA, *et al*. Plant mediated fabrication of silver nanoparticles, process optimization, and impact on tomato plant. Sci Rep. 2023;13(1):18048. doi: 10.1038/s41598-023-45038-x, PMID 37872286.
8. Nayak D, Ashe S, Rauta PR, Kumari M, Nayak B. Bark extract mediated green synthesis of silver nanoparticles: evaluation of antimicrobial activity and antiproliferative response against osteosarcoma. Mater Sci Eng C Mater Biol Appl. 2015;58:44-52. doi: 10.1016/j.msec.2015.08.022, PMID 26478285.
9. Bibi S, Abu-Dieyeh MH, Al-Ghouti MA. Biosynthesis of silver nanoparticles from macroalgae Hormophysa triquetra and investigation of its antibacterial activity and mechanism against pathogenic bacteria. Sci Rep. 2025;15(1):2476. doi: 10.1038/s41598-024-84760-y, PMID 39833251.
10. Muhaimin M, Chaerunisaa AY, Rostinawati T, Amalia E, Hazrina A, Nurhasanah S. A review on nanoparticles of Moringa oleifera extract: preparation, characterization, and activity. Int J Appl Pharm. 2023;15(4):43-51. doi: 10.22159/ijap.2023v15i4.47709.
11. Tareq SM, Boutchuen A, Roy S, Zimmerman D, Jur G, Bathi JR, *et al*. A dynamic light scattering approach for detection of nanomaterials in Tennessee River. Water Resour Res. 2021;57(8):WR028687:e2020. doi: 10.1029/2020WR028687.
12. Antony E, Sathiavelu M, Arunachalam S. Synthesis of silver nanoparticles from the medicinal plant Bauhinia acuminata and Biophytum sensitivum – a comparative study of its biological activities with plant extract. Int J Appl Pharm. 2016;9(1):22-9. doi: 10.22159/ijap.2017v9i1.16277.
13. Kamble S, Govind K Lohiya, Priyanka Sharnangat, Monika Kherade, Tirupati Rasala, Janhavi Indurkar, *et al*. Investigating the anti-cancer properties of a newly synthesized metal-quercetin nanocomplex in the context of cervical cancer. Asian J Pharm Clin Res. Apr 2025;18(4):223-9. doi: 10.22159/ajpcr.2025v18i4.53670.
14. Sevinc-Sasmaz C, Erci F, Torlak E, Yöntem M. Characterization of silver nanoparticles synthesized using Hypericum perforatum L. and their effects on Staphylococcus aureus. Microsc Res Tech. 2025 Mar 23;88(8):2321-32. doi: 10.1002/jemt.24862, PMID 40121669.
15. Kaurani P, Hindocha AD, Jayasinghe RM, Pai UY, Batra K, Price C. Effect of addition of titanium dioxide nanoparticles on the antimicrobial properties, surface roughness and surface hardness of polymethyl methacrylate: a Systematic Review. F1000Res. 2023;12:577. doi: 10.12688/f1000research.130028.1, PMID 37424742.
16. Punz B, Christ C, Waldl A, Li S, Liu Y, Johnson L, *et al*. Nano-scaled advanced materials for antimicrobial applications – mechanistic insight, functional performance measures, and potential towards sustainability and circularity. Environ Sci Nano. 2025;12(3):1710-39. doi: 10.1039/D4EN00798K.
17. Dass K, Mariappan P, Ramya P, Prakash N. Green synthesis of silver nanoparticles for mosquito control: a review of larvicidal activity from plant extracts. UP J Zool. 2024;45(22):242-66. doi: 10.56557/upjoz/2024/v45i224677.